

Ultrahigh-Q mechanical oscillators through optical trapping

D.E. Chang,¹ K.-K. Ni,² O. Painter,³ and H.J. Kimble²

¹*Institute for Quantum Information,*

California Institute of Technology, Pasadena, CA 91125

²*Norman Bridge Laboratory of Physics 12-33,*

California Institute of Technology, Pasadena, CA 91125

³*Thomas J. Watson, Sr., Laboratory of Applied Physics,*

California Institute of Technology, Pasadena, CA 91125

(Dated: January 4, 2019)

Abstract

Rapid advances are being made toward optically cooling a single mode of a micro-mechanical system to its quantum ground state and observing quantum behavior at macroscopic scales. Reaching this regime in room-temperature environments requires a stringent condition on the mechanical quality factor Q_m and frequency f_m , $Q_m f_m \gtrsim k_B T_{\text{bath}}/h$, which so far has been marginally satisfied only in a small number of systems. Here we propose and analyze a new class of systems that should enable unprecedented $Q_m f_m$ values. The technique is based upon using optical forces to “trap” and stiffen the motion of a tethered mechanical structure, thereby freeing the resultant mechanical frequencies and decoherence rates from underlying material properties.

The coupling of a high- Q mode of a micro-mechanical oscillator to an optical cavity has emerged as a promising route toward observing quantum behavior at macroscopic scales [1]. This opto-mechanical interaction is being used, for example, to optically cool a mechanical mode toward its quantum ground state [1]. A fundamental requirement is that the optical cooling rate must exceed the re-heating rate due to environmental coupling. This translates into a condition that must be satisfied for the product of the quality factor Q_m and frequency f_m of the mechanical mode, $Q_m f_m \gtrsim k_B T_{\text{bath}}/h$, where h is Planck’s constant. In a room-temperature bath, this condition is marginally satisfied only in a small number of current experiments [2]. Achieving large Q -frequency products is also crucial to extending the coherence time of the mechanical system and observing coherent quantum dynamics.

In this Letter, we propose a class of systems that should enable unprecedented Q -frequency products. The approach is based upon optically “trapping” a tethered membrane with low natural mechanical frequency in the anti-node of a strong optical standing wave (see Figs. 1a,b) [3]. Here, the relatively large dielectric disk supported by the thin tethers is attracted to the anti-node, leading to an optical stiffening of its flexural modes [4, 5]. We show that under realistic conditions, the re-normalized mode frequencies can be significantly enhanced over the values expected under material stresses alone. Of particular interest is the “center-of-mass” (CM) mode, where the disk oscillates in the optical potential with negligible internal bending and stresses. This mode can exhibit extremely large Q -frequency products due to the absence of mechanical dissipation through internal friction and viscosity.

Our approach to achieving long coherence times builds upon previous proposals, which suggested that the CM mode of an optically levitated nanosphere can be largely decoupled from its environment and enable quantum opto-mechanics in room-temperature environments [6–8]. Compared to the nanosphere, our approach has two significant advantages. First, the dielectric nanosphere scatters light omni-directionally, leading to heating of the CM motion via photon recoil. Suppression of recoil heating to reach the quantum regime requires spheres with sub-wavelength volumes, $V/\lambda^3 \ll 1$ [7]. In contrast, the planar membrane primarily couples together the forward- and backward-propagating components of the trapping beam, strongly reducing recoil heating even for large systems. Second, these membranes can be fabricated using well-established techniques that already yield excellent mechanical and optical properties in a number of experiments [2, 9, 10]. Our proposal thus shows how the ideas of optical levitation can be brought to bear upon “conventional” and

practically deployable opto-mechanical systems to yield remarkable coherence times.

We begin by considering the mechanical modes of a free, thin circular membrane of radius a in the absence of any tethers. In equilibrium, the membrane is situated at $z = 0$, in the anti-node of an optical standing wave $E(z) \propto \cos kz$ (see Fig. 1b). For simplicity, we assume that the membrane in equilibrium is rotationally symmetric, with an additional reflection symmetry around $z = 0$ and a thickness profile along the transverse direction r given by $d(r)$. The optical field polarizes the dielectric disk, yielding a gradient force trap around $z = 0$. Absent any internal forces, the optical trap for a thin membrane ($d \ll \lambda$) provides a thickness-independent trap frequency given by $\omega_{\text{opt}}(r) = \left(\frac{2k^2 I(r)(\epsilon-1)}{\rho c} \right)^{1/2}$. Here $I(r)$ is the local beam intensity (also assumed to be rotationally symmetric), $k = 2\pi/\lambda$ is the optical wavevector, ρ is the mass density, and ϵ is the dielectric constant. Now including the internal stresses, the equation of motion for the non-uniform disk can be found by generalizing that of a uniform thin disk (constant d) [11]. We find that the mechanical displacement field from equilibrium, $\zeta(x, y)$, obeys

$$\begin{aligned} \frac{\partial^2 \zeta}{\partial t^2} = & -\omega_{\text{opt}}^2(r)\zeta - \frac{E}{12\rho(1-\sigma^2)d(r)} \left(\nabla^2 (g(r)\nabla^2 \zeta) \right. \\ & \left. -(1-\sigma)(\zeta_{yy}g_{xx} + \zeta_{xx}g_{yy} - 2\zeta_{xy}g_{xy}) \right), \end{aligned} \quad (1)$$

where E, σ are the Young's modulus and Poisson's ratio, respectively, $g(r) = d(r)^3$, and $\zeta_{yy} = \partial^2 \zeta / \partial y^2$, etc. Here and in the following ∇^2 is understood to be the Laplacian in the transverse plane. Defining n and l to be the normal and tangential directions to the edge of the disk, and θ as the local angle between x and n , the boundary conditions at the edge of a free disk are

$$\begin{aligned} 0 = & \frac{\partial}{\partial n} (g\nabla^2 \zeta) + (1-\sigma) \times \\ & \left[\frac{\partial}{\partial l} (-g\zeta_{xy} \cos 2\theta + (g/2) \sin 2\theta (\zeta_{xx} - \zeta_{yy})) \right. \\ & \left. + \cos \theta (\zeta_{yy}g_x - \zeta_{xy}g_y) + \sin \theta (\zeta_{xx}g_y - \zeta_{xy}g_x) \right], \\ 0 = & \nabla^2 \zeta + (1-\sigma) \times \\ & (2\zeta_{xy} \sin \theta \cos \theta - \zeta_{yy} \cos^2 \theta - \zeta_{xx} \sin^2 \theta). \end{aligned} \quad (2)$$

It is helpful to first consider the normal modes of a disk of uniform thickness d in absence of optical forces. Due to the rotational symmetry, we seek solutions of the form $\zeta(x, y) = f(r) \cos m\theta e^{-i\omega_m t}$, which reduces Eqs. (1) and (2) to differential equations involving $f(r)$

alone. The spatial modes are indexed by the number of nodal diameters and circles, (m, n) . The lowest few modes of a disk are shown in Figs. 1c,d. For our numerical results we take material parameters $E = 270$ GPa, $\sigma = 0.25$, $\rho = 2.7$ g/cm³, $\epsilon = 4$ corresponding to stoichiometric silicon nitride [2], and an operating wavelength of $\lambda = 1$ μ m. The fundamental $(2, 0)$ mode has natural frequency $\omega_{m,\text{nat}}^{(2,0)}/2\pi \approx 0.25 \frac{d}{a^2} \sqrt{\frac{E}{\rho(1-\sigma^2)}}$, or $\omega_{m,\text{nat}}^{(2,0)}/2\pi \approx 190$ kHz for a disk of dimensions $a = 20$ μ m, $d = 30$ nm. There is a trivial solution corresponding to the CM mode with $f(r) = \text{constant}$ and zero frequency.

In the presence of an optical field with uniform transverse profile, $I(r) = I_0$, one can readily verify that the natural spatial modes $f_{\text{nat}}^{(m,n)}(r)$ remain eigenmodes of Eq. (1), but with re-normalized mechanical frequencies given by $\omega_m^{(m,n)}(I_0) = \sqrt{\omega_{\text{opt}}^2(I_0) + (\omega_{m,\text{nat}}^{(m,n)})^2}$. There are two important features to note about these solutions. First, the CM mode is now a non-trivial solution with frequency $\omega_m^{\text{CM}} = \omega_{\text{opt}}$, but still retains a uniform spatial profile. Second, the frequencies of all the flexural modes increase as well, with the CM mode remaining the lowest in frequency (see Fig. 1c).

The absence of spatial deformations in the CM mode oscillation has profound implications for the mechanical quality factor. In particular, none of the mechanical energy is stored in internal strains, thus eliminating dissipation due to internal friction or viscosity. Instead, the energy is stored in the lossless optical potential. To quantify this effect, we consider the influence of optical trapping on a specific loss channel, thermoelastic damping. We focus on thermoelastic damping because a) it can be analytically modelled [11, 12], b) it is a fundamental limit to the quality factor even if the device is “perfect” [12], and c) a number of micro-mechanical systems are approaching the thermoelastic limit [13, 14]. We emphasize, however, that our conclusions are quite general to any internal dissipation process.

Thermoelastic damping arises because realistic materials have a non-zero coefficient of thermal expansion. The flexural motion of a system creates local volume changes that then lead to temperature gradients and heat flow. Mechanical energy must be expended to drive this heat flow, leading to a finite Q_m . We make two simplifying assumptions to the general thermoelastic equations [11, 12], which are well-justified in our system. First, we assume that the thermoelastic coupling is weak, so that the spatial modes determined by Eq. (1) are not altered to lowest order. Second, the strains vary most rapidly along the thin direction of the disk, and thus we ignore the small temperature gradients created in the transverse direction. The temperature field is given by $T(x, y, z, t) = T_{\text{bath}} + \Delta T(x, y, z, t)$, where ΔT

satisfies the driven heat equation

$$\left(c_V \frac{\partial}{\partial t} - \kappa_{\text{th}} \frac{\partial^2}{\partial z^2}\right) \Delta T = \frac{E\alpha T_{\text{bath}} z}{3(1-2\sigma)} \frac{\partial}{\partial t} \nabla^2 \zeta \quad (3)$$

with boundary conditions $\partial \Delta T / \partial z = 0$ at $z = \pm d(r)/2$. Here c_V is the heat capacity per unit volume, κ_{th} is the thermal conductivity, and α is the volumetric thermal expansion coefficient. For a particular mechanical eigenmode ζ , the amount of work done in driving the heat flow over one cycle is

$$\Delta W \approx -\frac{\kappa_{\text{th}}}{T_{\text{bath}}} \int_0^{2\pi/\omega_m} dt \int d^3\mathbf{r} \Delta T(\mathbf{r}) (\Delta T)_{zz}, \quad (4)$$

and the thermoelastically limited quality factor is $Q_{m,\text{th}} = 2\pi W / \Delta W$, where W is the total mechanical energy. As a useful comparison, one can apply these equations to the flexural modes of conventional square, clamped membranes [2, 9]. In the relevant limit where the thickness d is much smaller than the characteristic thermal diffusion length $l_d = \sqrt{\kappa_{\text{th}}/c_V \omega_m}$, one finds a thermoelastically limited Q -frequency product for an unstressed membrane given by $Q_{m,\text{th}} f_m = \frac{45\kappa_{\text{th}}}{\pi E d^2 T_{\text{bath}} \alpha^2} \frac{1-\sigma}{1+\sigma}$, independent of the mode frequency and transverse size. For stoichiometric SiN films of thickness $d = 30$ nm, $Q_{m,\text{th}} f_m \approx 10^{14}$ Hz at room temperature, which only marginally exceeds the fundamental limit $k_B T_{\text{bath}} / h \approx 6 \times 10^{12}$ Hz needed for ground-state cooling. The Q -frequency product has further relevance as it is proportional to the number of coherent oscillations that the system can undergo before a single phonon is exchanged with the thermal bath, $N_{\text{th}}^{(\text{osc})} = Q_{m,\text{th}} f_m h / (2\pi k_B T_{\text{bath}})$ ($N_{\text{th}}^{(\text{osc})} \sim 2.5$ for the square membrane described above). A large value is necessary if one wants to observe coherent quantum dynamics.

We now examine thermoelastic damping in the case of our free disk. Clearly, if $\omega_{\text{opt}}(r)$ is spatially uniform, the CM mode has no internal strains and thermoelastic processes would contribute zero dissipation. The transition to this regime can be understood by considering a varying transverse beam profile. For concreteness, suppose that the trapping beam has a Gaussian transverse profile with beam waist w , $I(r) = I_0 e^{-2r^2/w^2}$ (for now, we ignore possible corrections due to distortion as the beam diffracts around the disk). Intuitively, when w is finite, the pure CM motion becomes mixed with internal bending, as internal stresses must compensate for the unbalanced optical forces at the disk center versus its edge (we still refer to this mixed mode as the “CM”). The mixing gives rise to a finite Q -frequency product, whose value rises by a) using smaller disk radius, to make it stiffer to bending, or b) using larger beam waists, to homogenize the optical force across the disk.

These effects are illustrated in Fig. 2. First, in Fig. 2a, the peak intensity I_0 is fixed to a corresponding peak trap frequency $\omega_{\text{opt}}(I_0)/2\pi = 1$ MHz, and the beam waist w is varied. Here the Q -frequency product of the CM mode is plotted versus w/a , for two different disk sizes $a = 10 \mu\text{m}$ and $a = 20 \mu\text{m}$ (each of thickness $d = 30$ nm). The corresponding mode frequencies ω_m are plotted as well. As expected, the Q -frequency product increases for large w/a (even as ω_m saturates) and smaller disk size. There is also a less interesting regime where the Q -frequency product improves in the limit of very small w/a , at the expense of vanishing frequency, as the total optical restoring force becomes negligible to bend the disk. Significantly, the Q -frequency product can exceed the “natural” thermoelastic limit of the internal modes by several orders of magnitude even for moderate values of w/a . The direct correlation between the achievable Q -frequency product and the internal bending can be seen in Fig. 2b, where the CM mode amplitudes $f(r)$ are plotted for various values of w/a . In Fig. 2c, we plot the Q -frequency product and ω_m for fixed values of w/a but varying the peak intensity I_0 . Here the Q -frequency product decreases with increasing intensity, as the larger difference in optical forces across the size of the disk mixes in more internal motion.

Thus far our results are equally valid whether the membrane is trapped in free space or within a Fabry-Perot cavity, but a cavity is needed to enable optical cooling and reach the quantum regime [15, 16]. The membrane diffracts and scatters the cavity light, which introduces two important effects. First, the optical mode will no longer be Gaussian, and the new optical mode accommodated by the mirrors and the corresponding optical forces must be determined. Second, scattering out of the cavity reduces the cavity finesse, and the associated photon recoil acts as a stochastic force that heats the membrane motion. To calculate the cavity modes in the presence of the membrane, we use a modified Fox-Li propagation technique [17]. Specifically, the electric field is treated within the scalar paraxial approximation, which allows a beam front $E(x, y)$ originating at one of the cavity mirrors to be propagated to the membrane via fast Fourier transform (or discrete Hankel transform, for our rotationally symmetric system). This approximation is justified by noting that the disk should primarily diffract light at small angles $\theta \lesssim (ka)^{-1}$ around the z -axis. At the membrane location, the propagated beam front experiences reflection and transmission amplitudes $r(x, y)$, $t(x, y)$, respectively, generating new phase fronts in each direction (note that the original technique of Ref. [17] only accounts for transmission). For the case of a non-uniform disk, we approximate $r(x, y), t(x, y)$ with the formulas for an infinite thin dielectric sheet

of uniform thickness, replacing the uniform thickness $d \rightarrow d(x, y)$ with the local thickness. The new reflected and transmitted beam fronts can then be propagated back to the mirrors via another Hankel transform. Properly summing all of the combinations of reflection and transmission enables one to calculate the field buildup or the cavity eigenmodes.

We now discuss the effect of the membrane on the cavity finesse. As realistic parameters, we consider a membrane placed symmetrically in the center of an optical cavity of length $L = 1.99$ cm with spherical mirrors having radii of curvature $R_c = 1$ cm and perfect reflectivity (such that the entire cavity linewidth κ is attributable to scattering from the membrane). The transverse extent of the spherical mirror surfaces is $r_m = 0.95$ mm, *i.e.*, all portions of the beam front with $x^2 + y^2 > r_m^2$ are scattered out and set to zero upon reflection at the mirror. An empty cavity in this configuration yields a Gaussian mode of waist $w_0 \approx 15$ μm in the center. In Fig. 3a, we plot the membrane-limited cavity finesse $F_{\text{mem}} \equiv \pi c / \kappa L$ for a membrane of uniform thickness $d = 30$ nm and varying radius a (black circles). Clearly, cavity losses are negligible when the nominal waist is small compared to the disk radius, $w_0/a \lesssim 1$. In the regime $w_0/a \gtrsim 1$, however, the finesse rapidly drops, which is attributable to scattering by the hard edges of the disk. This effect is strongly reduced by “softening” or apodizing the disk edge [18]. In Fig. 3a (red circles), we also plot the finesse for a membrane whose thickness $d(r) = d_0(1 - (r/a)^2)^2$ tapers down to zero at the edge, where $d_0 = 30$ nm is the maximum thickness. Remarkably, the apodization can improve the cavity finesse by several orders of magnitude. The modification of the cavity modes by the membrane is illustrated in Fig. 3b, where we plot the transverse profile at the membrane position for some representative apodized disk sizes.

We find the CM eigenmodes of the apodized disk by using Eq. (1), where the optical potential $\omega_{\text{opt}}(r)$ is now evaluated using the modified cavity mode profiles. The thermoelastic limit is subsequently calculated using Eqs. (3) and (4). In Fig. 3c, the number of oscillations $N_{\text{th}}^{(\text{osc})}$ due to thermoelastic damping is plotted (in black). Here the circulating intra-cavity power is chosen such that the CM frequency is fixed at $\omega_m/2\pi = 0.5$ MHz. We next consider the effect of photon recoil heating. We assume that each scattered photon contributes the maximum possible momentum kick of $\hbar k$ along the z -axis, giving rise to a momentum diffusion process $d\langle p_z^2 \rangle / dt = (\hbar k)^2 R_{\text{sc}}$ [7], where R_{sc} is the photon scattering rate. Converting this expression into a jump rate, it can be shown that the number of coherent oscillations

before a jump in the phonon number can be written as

$$N_{\text{sc}}^{(\text{osc})} = \frac{1}{2\pi} \frac{V}{V_c} \frac{\omega_0}{\kappa} \frac{\omega_m^2}{k^2 I_{\text{max}}/\rho c}. \quad (5)$$

Here I_{max} is the maximum cavity intensity (which in general does not need to be at the center of the membrane due to mode distortion), $\omega_0 = ck$, V is the volume of the disk, and V_c is the cavity mode volume. Assuming that the cavity mode is not significantly distorted and that the beam waist $w_0 \gtrsim a$ such that the entire membrane experiences the optical force, one can approximate $\frac{\omega_m^2}{k^2 I_{\text{max}}/\rho c} \sim 1$ and $V_c \sim \pi w_0^2 L/4$. In this case the number of coherent oscillations scales roughly as $N_{\text{sc}}^{(\text{osc})} \sim \frac{kV}{w_0^2} F_{\text{mem}}$. Note that this result is purely geometric in nature and also scales directly with the cavity finesse (which itself depends on V). In Fig. 3c, we plot $N_{\text{sc}}^{(\text{osc})}$ for the apodized disk (in red). Combining the effects of thermoelastic damping and recoil heating, the total number of coherent oscillations is given by $N_{\text{tot}}^{(\text{osc})} = (N_{\text{sc}}^{(\text{osc})-1} + N_{\text{th}}^{(\text{osc})-1})^{-1}$ (blue curve). It can be seen that an apodized disk of radius $r \sim 9 \mu\text{m}$ can support a coherence time of $N_{\text{tot}}^{(\text{osc})} \sim 2000$ in a room temperature environment. This is ~ 10 times larger than that of a much smaller levitated nanosphere of 50 nm radius [7].

While we have thus far considered a levitated membrane, as a realistic implementation we propose a tethered membrane such as that shown in Fig. 1a. Here, the tethers provide an extremely weak restoring force for the “CM” motion of the central disk, which allows the CM frequency of the disk to be strongly enhanced by optical forces. Additional calculations show that one recovers the previous results for the free disk in the limit that the tether mass m_t is small compared to the disk mass m_{disk} . In particular, when the CM frequency is far from any tether resonances, the motion of the tethers comprises a small fraction $\sim m_t/m_{\text{disk}}$ of the total system energy, and contributes a correspondingly small amount of dissipation.

Finally, we emphasize that although we have focused on thermoelastic losses in the above calculations, we expect similar improvements for any other internal damping mechanism (*e.g.*, a small imaginary component of the Young’s modulus E). The key idea is that it is possible to circumvent natural material limits of mechanical damping by storing energy in a lossless optical field rather than the internal strain. By making the ratio of these energies large, $U_{\text{opt}}/U_{\text{mech}} \gg 1$, any internal losses can be suppressed by a corresponding degree. This fundamental observation allows one to design a novel class of mechanical systems that can be fabricated and deployed using conventional techniques, yet yield Q -frequency products

that are several orders of magnitude higher than previous systems. We believe that this work will stimulate further investigation into the relationship between optical forces and material dissipation in a number of systems where the mechanical motion can be strongly renormalized by light [5, 19]. Furthermore, we anticipate that such studies will open up interesting possibilities for quantum manipulation of mechanical systems in room-temperature environments.

The authors thank Dal Wilson and Richard Norte for many helpful discussions. DEC acknowledges support from the NSF (Grant No. PHY-0803371) and the Gordon and Betty Moore Foundation through Caltech's Center for the Physics of Information (CPI). KN acknowledges support from the CPI. HJK and OJP acknowledge support from the DARPA ORCHID program. HJK also acknowledges support from the NSF and DoD NSSEFF.

-
- [1] A. Cleland, *Nature Phys.* **5**, 458 (2009).
 - [2] D. J. Wilson, C. A. Regal, S. B. Papp, and H. J. Kimble, *Phys. Rev. Lett.* **103**, 207204 (pages 4) (2009).
 - [3] A. Ashkin, *Optical Trapping and Manipulation of Neutral Particles Using Lasers: a Reprint Volume with Commentaries* (World Scientific, 2007).
 - [4] V. B. Braginsky and S. P. Vyatchanin, *Phys. Lett. A* **293**, 228 (2002).
 - [5] T. Corbitt, Y. Chen, E. Innerhofer, H. Müller-Ebhardt, D. Ottaway, H. Rehbein, D. Sigg, S. Whitcomb, C. Wipf, and N. Mavalvala, *Phys. Rev. Lett.* **98**, 150802 (2007).
 - [6] K. G. Libbrecht and E. D. Black, *Phys. Lett. A* **321**, 99 (2004).
 - [7] D. E. Chang, C. A. Regal, S. B. Papp, D. J. Wilson, J. Ye, O. Painter, H. J. Kimble, and P. Zoller, *Proc. Natl. Acad. Sci. USA* **107**, 1005 (2010).
 - [8] O. Romero-Isart, M. L. Juan, R. Quidant, and J. I. Cirac, *New J. Phys.* **12**, 033015 (2010).
 - [9] J. D. Thompson, B. M. Zwickl, A. M. Jayich, F. Marquardt, S. M. Girvin, and J. G. E. Harris, *Nature* **452**, 72 (2008).
 - [10] J. C. Sankey, C. Yang, B. M. Zwickl, A. M. Jayich, and J. G. E. Harris, *Nature Phys.* **6**, 707 (2010).
 - [11] L. D. Landau and E. M. Lifshitz, *Theory of elasticity, 3rd ed.* (Butterworth-Heinemann, Boston, 1986).

- [12] R. Lifshitz and M. L. Roukes, Phys. Rev. B **61**, 5600 (2000).
- [13] S. S. Verbridge, J. M. Parpia, R. B. Reichenbach, L. M. Bellan, and H. G. Craighead, J. Appl. Phys. **99**, 124304 (pages 8) (2006).
- [14] J. E.-Y. Lee and A. A. Seshia, Sens. Actuators A **156**, 28 (2009).
- [15] I. Wilson-Rae, N. Nooshi, W. Zwerger, and T. J. Kippenberg, Phys. Rev. Lett. **99**, 093901 (pages 4) (2007).
- [16] F. Marquardt, J. P. Chen, A. A. Clerk, and S. M. Girvin, Phys. Rev. Lett. **99**, 093902 (pages 4) (2007).
- [17] A. G. Fox and T. Li, IEEE J. Quantum Electron. **4**, 460 (1968).
- [18] M. Born, E. Wolf, and A. B. Bhatia, *Principles of optics: electromagnetic theory of propagation, interference and diffraction of light* (Cambridge University Press, 2000).
- [19] J. Rosenberg, Q. Lin, and O. Painter, Nat. Photonics **3**, 478 (2009).

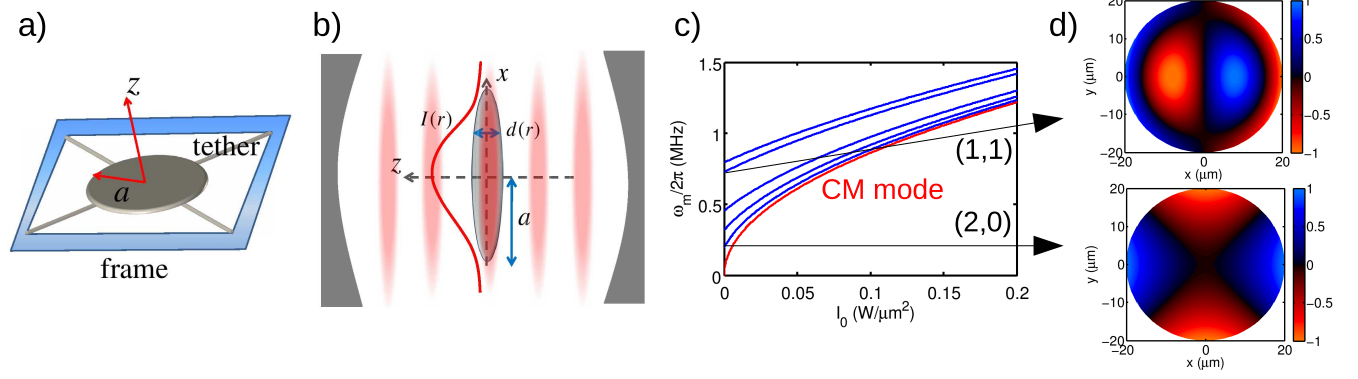


FIG. 1: a) Illustration of a tethered circular membrane supported by a solid frame. b) Side view of membrane inside a Fabry-Perot cavity. The membrane has radius a and a radial thickness profile $d(r)$. It is trapped in the anti-node of a standing optical field with transverse intensity profile $I(r)$. c) Normal mode frequencies of a SiN membrane of thickness $d = 30$ nm and radius $a = 20$ μm , trapped in a plane standing wave of intensity I_0 . d) Motional amplitudes $\zeta(x, y)$ of selected internal modes $(m, n) = (2, 0)$ and $(m, n) = (1, 1)$, in arbitrary units.

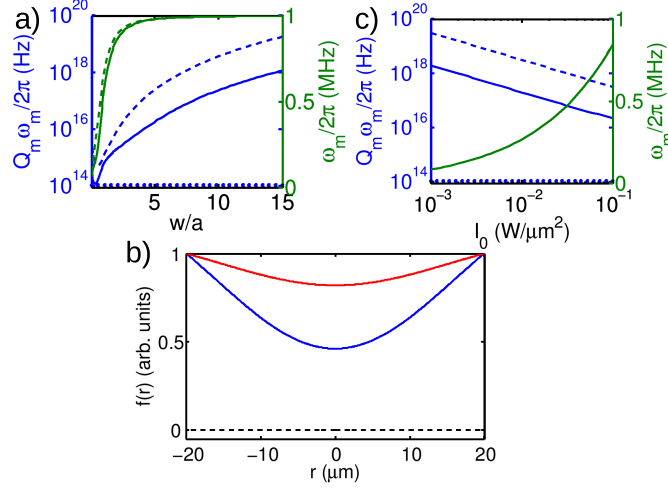


FIG. 2: a) Q -frequency product (blue curves) and mechanical frequency $\omega_m/2\pi$ (green) for an optically trapped disk, as a function of the beam waist to disk radius (w/a). The trap intensity is fixed such that $\omega_m/2\pi = 1$ MHz in the plane wave limit. The disk thickness is $d = 30$ nm, and the radii are $a = 20 \mu\text{m}$ (solid curves) and $a = 10 \mu\text{m}$ (dashed). The Q -frequency product of a square clamped membrane of the same thickness (horizontal dotted line) is also shown for comparison. b) Spatial amplitudes of the CM motion $f(r)$ (in arbitrary units) for a disk radius $a = 20 \mu\text{m}$, under the same conditions as a). The blue and red curves correspond to $f(r)$ for ratios $w/a = 5$ and $w/a = 10$, respectively, while the dashed curve denotes the equilibrium plane. The negligible mixing of internal bending into the CM motion for $w/a = 10$ as compared to $w/a = 5$ is responsible for the higher Q -frequency product in the former case. c) Q -frequency product and mechanical frequency as a function of peak trap intensity I_0 , for disk radii $a = 20 \mu\text{m}$ (solid curves) and $a = 10 \mu\text{m}$ (dashed). The beam waist w is fixed to be $w = 5a$. The Q -frequency product of a square clamped membrane is denoted by the horizontal dotted line. In all cases, intrinsic losses for the material system are assumed to arise from thermoelastic damping only.

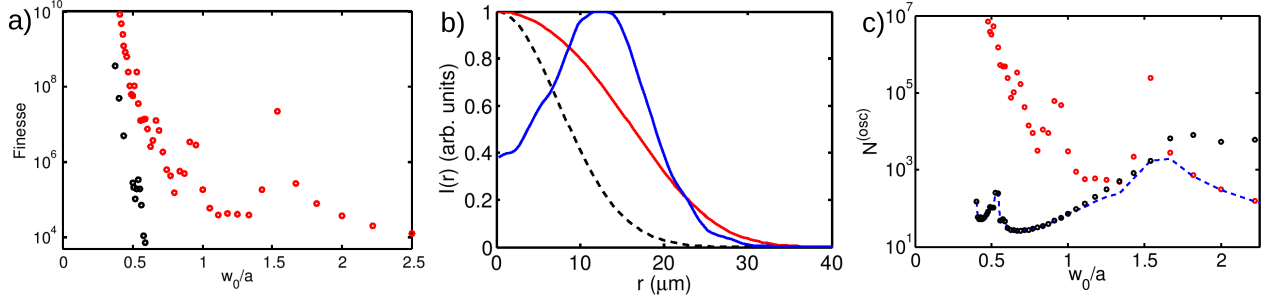


FIG. 3: a) Membrane-limited finesse F_{mem} of a Fabry-Perot cavity with a membrane in the middle. The black circles correspond to a flat membrane of uniform thickness $d = 30$ nm, while the red circles correspond to an apodized membrane with maximum thickness $d_0 = 30$ nm. The finesse is plotted as a function of the ratio of the empty-cavity beam waist w_0 to the membrane radius a . The cavity parameters are chosen such that $w_0 = 15 \mu\text{m}$. b) Intensity profiles (in arbitrary units) of cavity mode in the presence of an apodized membrane. The intensity profile is evaluated halfway between the two cavity mirrors. The cavity and membrane parameters are provided in the main text. The blue and red curves correspond to disk radii $a = w_0$ and $a = 2.5w_0$, respectively, while the dashed black curve is the Gaussian intensity profile for an empty cavity. c) The number of coherent oscillations of the CM motion of an apodized disk due to thermoelastic damping ($N_{\text{th}}^{(\text{osc})}$, black circles) and recoil heating ($N_{\text{sc}}^{(\text{osc})}$, red circles), as a function of disk radius and for fixed $w_0 = 15 \mu\text{m}$. Also plotted is the total number of coherent oscillations ($N_{\text{tot}}^{(\text{osc})}$, blue dashed curve), which is given by the sum in parallel of the individual contributions.